Dr. Konstantin MOCHALOV, Ph.D.,

Laboratory of Biophysics, Shemyakin & Ovchinnikov Institute of Bioorganic Chemistry, Russian Academy of Sciences

Moscow, Russia

Correlative technique for the high resolution multiparametric 3D analysis of optical and morphological properties in the bulk of nanomaterials

Correlative microscopy – combination of optical microspectroscopy and 3D high-resolution microscopies

The main demand is the study of exact relationship between the 3D morphology and optical properties of artificial and natural nanostructured objects.

It is clear that any single microscopy technology is unable to provide a comprehensive understanding of ultrastructure needed for these tasks and use of complementary multimodal microscopy techniques becomes the ultimate requirement.

Approaches to Correlative microscopy

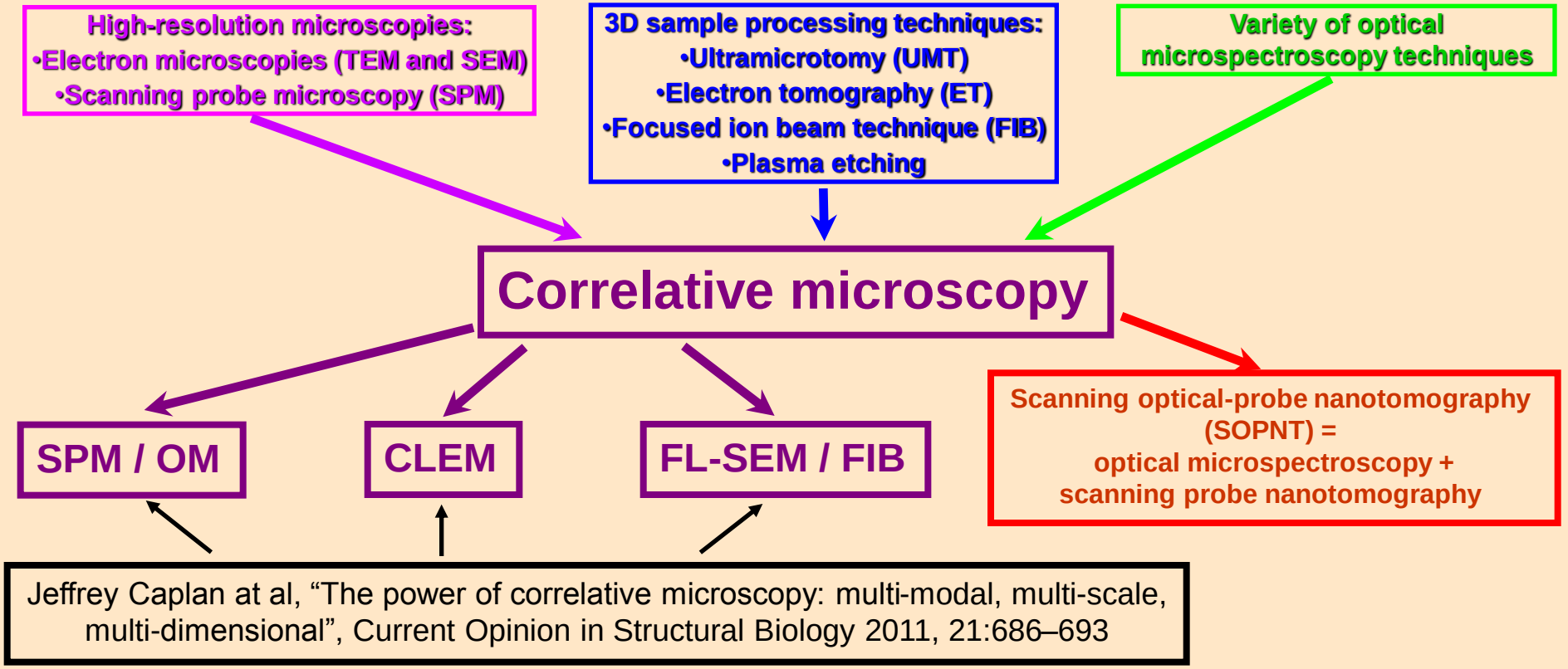

Jeffrey Caplan at al, “The power of correlative microscopy: multi-modal, multi-scale, multi-dimensional”, Current Opinion in Structural Biology 2011, 21:686–693

What is SPNT?

Scanning Probe Nanotomography (SPNT) – The combination of SPM and Ultramicrotomy

Background

Scanning probe microscopy
(surface analysis at nanoscale)

2D (XY)

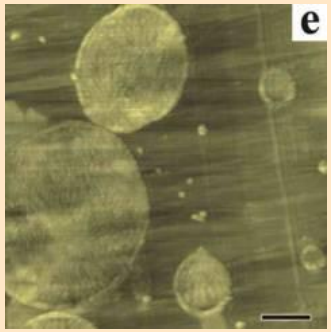

+

Ultramicrotomy
(ultrathin sectioning to 10 nm
At temperature from -190 to +20 C)

1D (Z)

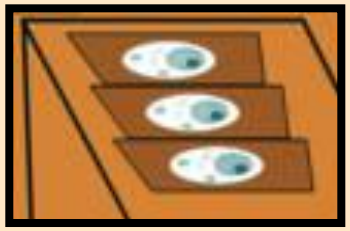

=

Scanning probe nanotomography

3D(XYZ)

What is SPNT?

Scanning Probe Nanotomography (SPNT) – The combination of SPM and Ultramicrotomy

CONCEPT: 3D image reconstruction with consecutive in situ SPM measurements performed immediately after each microtome section at the fresh surface of an untreated blockface - “slice-and-view” approach.

Scheme of combination of SPM and ultramicrotome

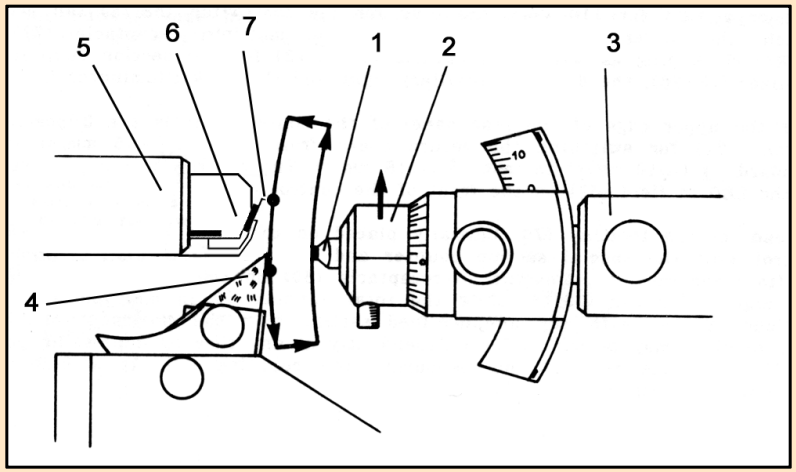

1 – sample, 2 – sample holder, 3 – moving ultramicrotome arm, 4 – ultramicrotome knife, 5 – SPM scanner, 6 – probe holder, 7 – SPM probe.

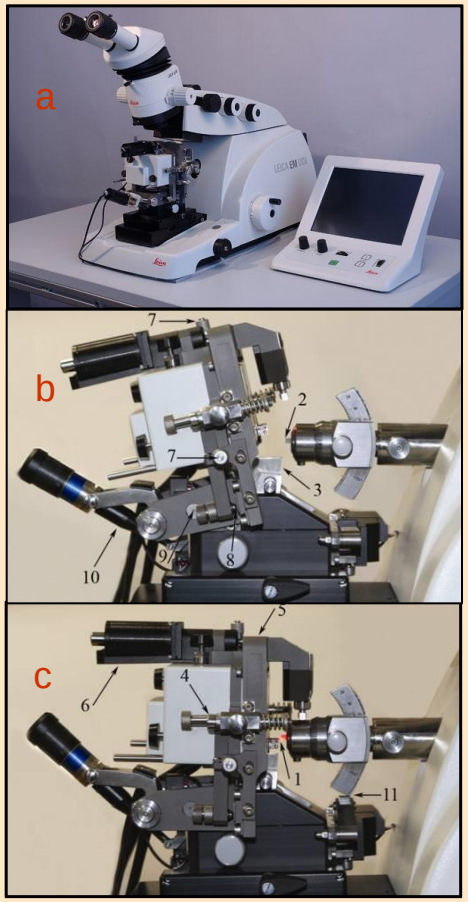

(a) Overview of SPNT setup
(b) SPM head in measuring and
(c) sectioning positions:
1) AFM probe;
2) sample;
3) ultramicrotome knife;
4) spring locks;
5) support platform;
6) stepper motor for probe approach;
7) positioning microscrews;
8) polysapphire plate;
9) support pivots;
10) motorized rear screw;
11) ultramicrotome arm support

The depth resolution of 3D reconstruction by SPNT is only limited by the thickness of sections removed from the blockface surface; it can be as fine as 10 nm. The maximum thickness of the reconstructed sample volume is, in principle, unlimited; analysis of specimens as thick as several micrometers is quite practicable.

SPMT is a nondestructive surface characterization technique for soft matter analysis, which may overcome some of the EM limitations because it does not induce any radiation damage of the sample surface.

What is SPNT?

SPNT - Results

Study of polymer and nanocomposite fibers

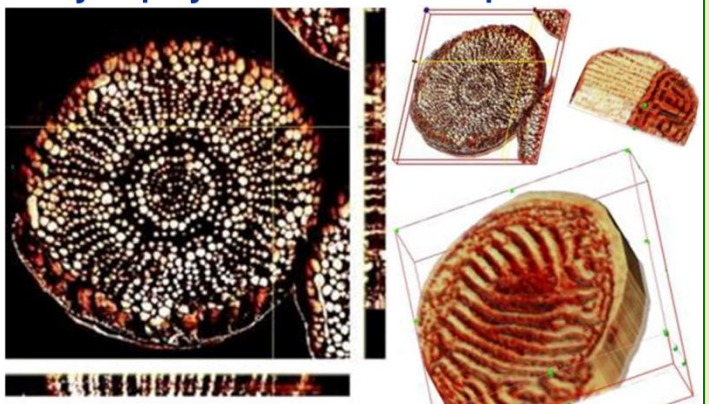

3D-reconstruction of carbon fibers (4x4x1μm) and polymer (PET/PE "islands-in-the-sea") fibers (32x32x1.5μm). Samples courtesy of Prof. J.P. Hinestrosa, Cornell University, USA

3D reconstruction of the polymer composite PA6/SAN

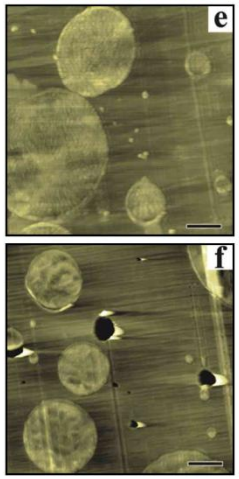

e) AFM – topography after the sectioning at -80°C.
f) AFM – topography at room temperature.
g, h) 3D reconstruction at -80°C: 6 cuts x 125 nm 7.9×6.2×0.75 μm и 2.0×2.0×0.75 μm, correspondingly.

A.E. Efimov et al, Soft Matter, 2012, 8, 9756, DOI:10.1039/c2sm26050f

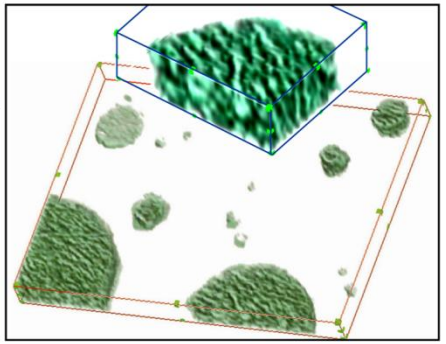

Surface visualization of the macromolecular content of the AFM 3D reconstructed cyanobacteria Synechococcus

Resulted volume image contains 432 × 398 × 6 voxels what corresponds to physical size of 2.7 × 2.5 × 0.15 um.

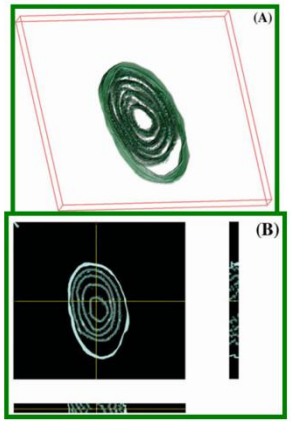

3D reconstruction of conductive nanocomposites

3D-reconstruction of the conductivity of the nanotube network inside the polystyrene/CNT composite, 1.8x1.6x0.26 um.
A. Alekseev, A. Efimov, K. Lu, J. Loos, Adv. Mater., 2009, 21, 4915

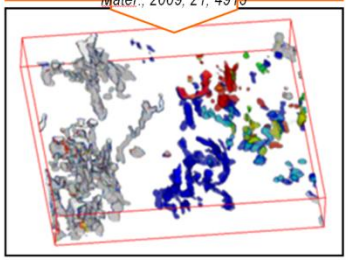

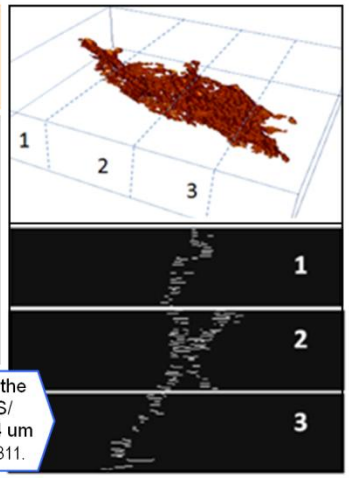

3D-reconstruction of the conductivity of the network of graphene flakes inside the PS/graphene nanocomposite, 2.5x2.5x0.34 um
A. Alekseev et al, Adv. Func. Mater., 2012, 22, 1311.

Scanning optical-probe nanotomography - optical and nearfield optical microspectroscopy & scanning probe nanotomography

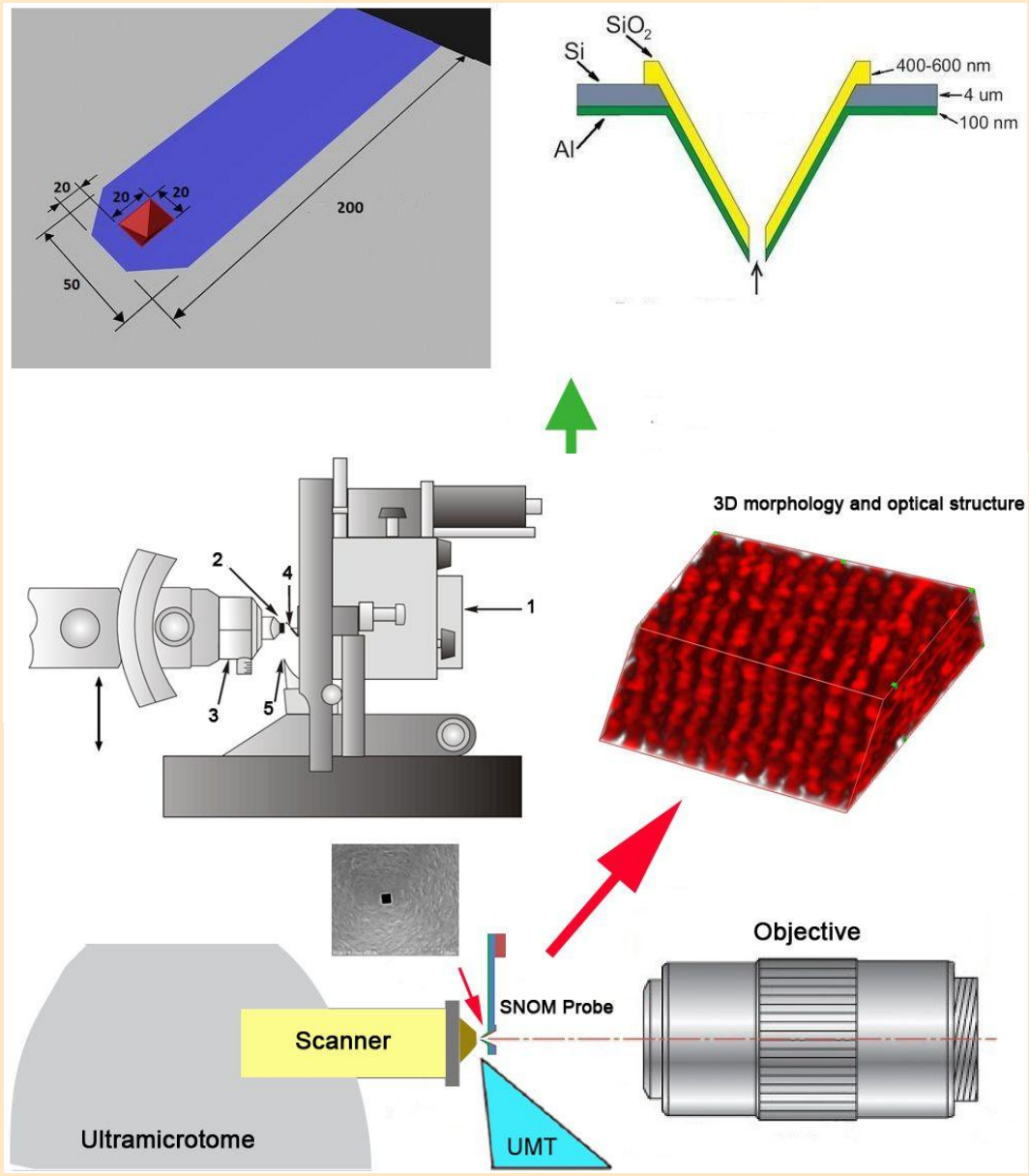

Standart setup for SNOM cantilever.

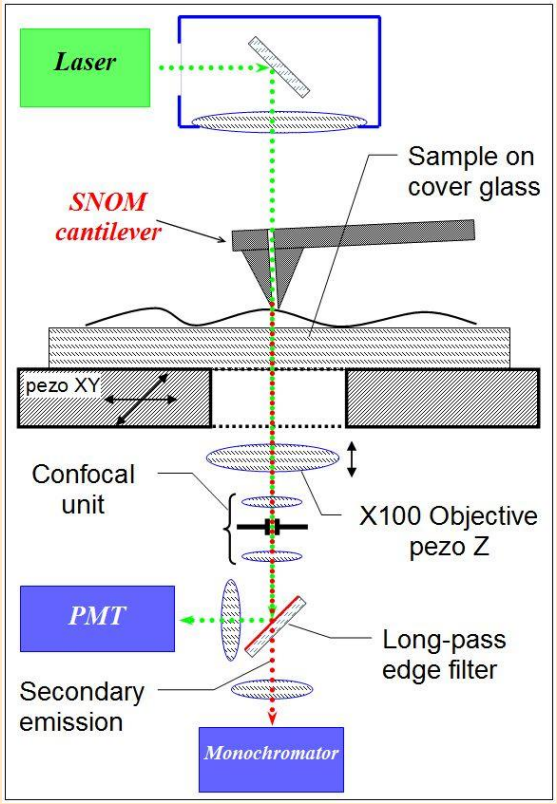

The main task of project - the development of single device for realization of SOPNT technique

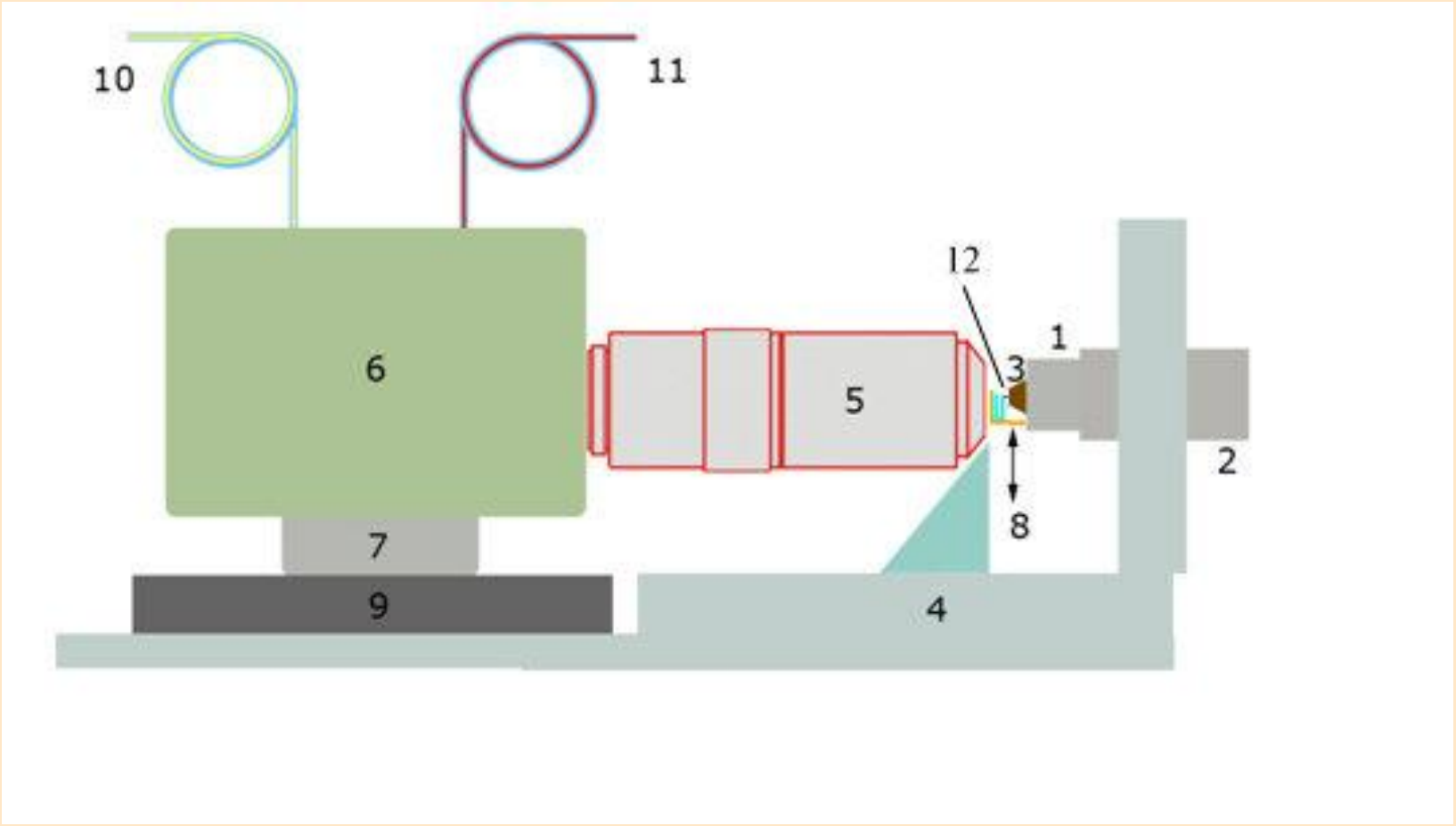

1 – sample holder with a piezotube XYZ scanner,
2 – movable ultramicrotome arm,
3 – sectioned sample,
4 – cryochamber,
5 – high-aperture optical objective,
6 – optical module,
7 – precise objective microposotioner,
8 – diamond knife,
9 – optical module platform,
10 – optical fiber for the laser excitation light,
11 – optical fiber guide to the monochromator.
12 – tuning fork-based AFM tip

Now SOPNT is the combination of two separate techniques in one exprimental procedure

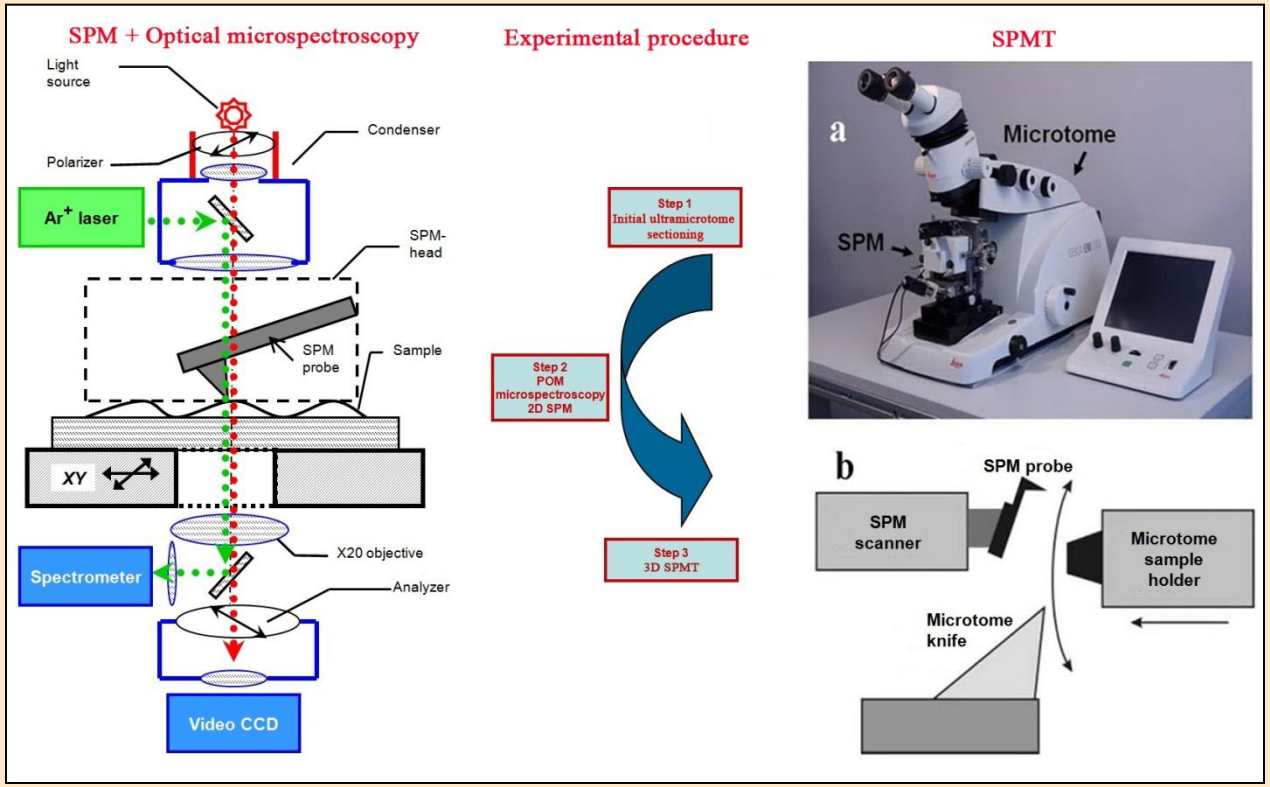

•The first step consists in initial ultramicrotome sectioning of the investigated sample deposited on a glass substrate in order to obtain a flat blockface surface for SPM/OM correlative microscopy.

•Then, the sample is transferred to a combined SPM/OM device for SPM and OM imaging and spectroscopic measurement.

•Finally the sample is transferred back to the SPNT system, where we locate the same surface areas on the block face by means of AFM and optical microscopy and then proceed with ultramicrotome sectioning of controlled uniform thickness and subsequent SPM measurements to obtain nanotomography 3D reconstruction.

SOPNT - Results

Analysis of the influence of aggregation of QDs embedded in a CLC matrix on their fluorescence characteristics

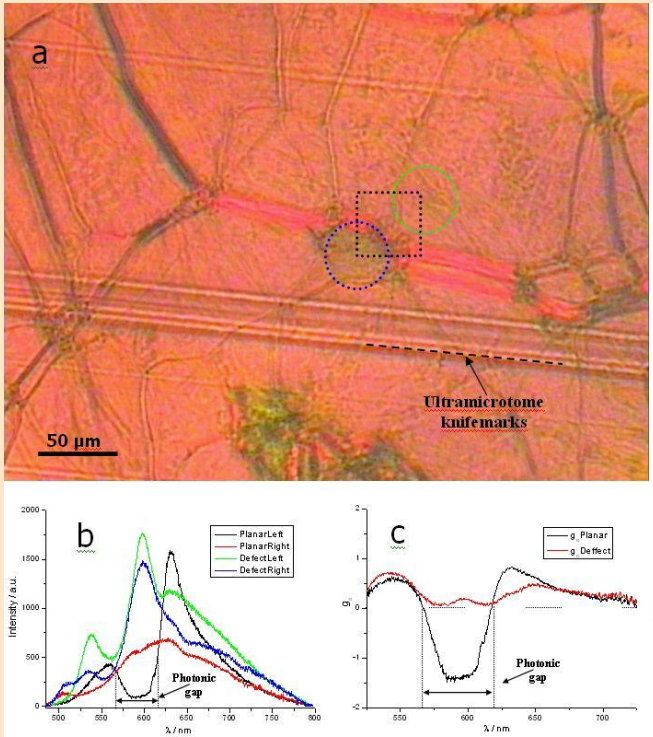

a) POM-image of the ultramicrotomed area of QD/CLC surface. Green circle marks area of “planar zone” fluorescence emission spectra acquisition. Blue circle marks area of “defect zone” fluorescence emission spectra acquisition. Black square – area scanned by AFM (Fig. 3a) including both planar and defect zones.
b) Right- and left-handed circularly polarized components of the fluorescence emission spectrum of QDs embedded in CLC-matrix.
c) Fluorescence dissymmetry factors of QDs embedded in CLC-matrix in planar and defect zones.

Structural analysis of the 2D and 3D distributions of QDs embedded in the cluster and homogeneous distribution zones of a CLC matrix

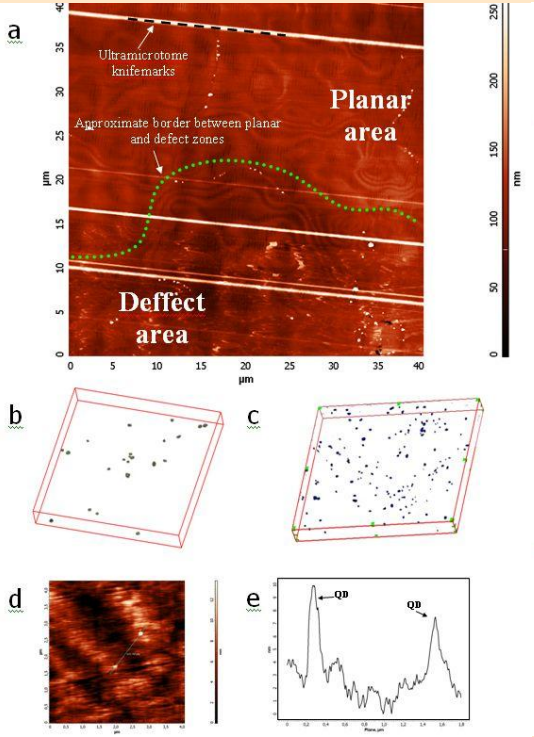

a) 2D AFM-image of QD/CLC sample area (40×40 µm) including both planar and defect zones
b) SPN 3D reconstruction of QD distribution in planar zone of QD/CLC structure. Dimensions of the reconstructed volume 5.0×5.0×0.7 µm.
c) SPN 3D of QD cluster distribution in defect zone of QD/CLC structure. Dimensions of the reconstructed volume 50×50×5.0 µm.
d) 2D AFM-image of planar zone of QD/CLC system with individual QDs – one of the images used for 3D reconstruction.
e) Cross-section of the AFM image 3d across the marked line.

Influence of single QDs within the CLC matrix on its planar structure

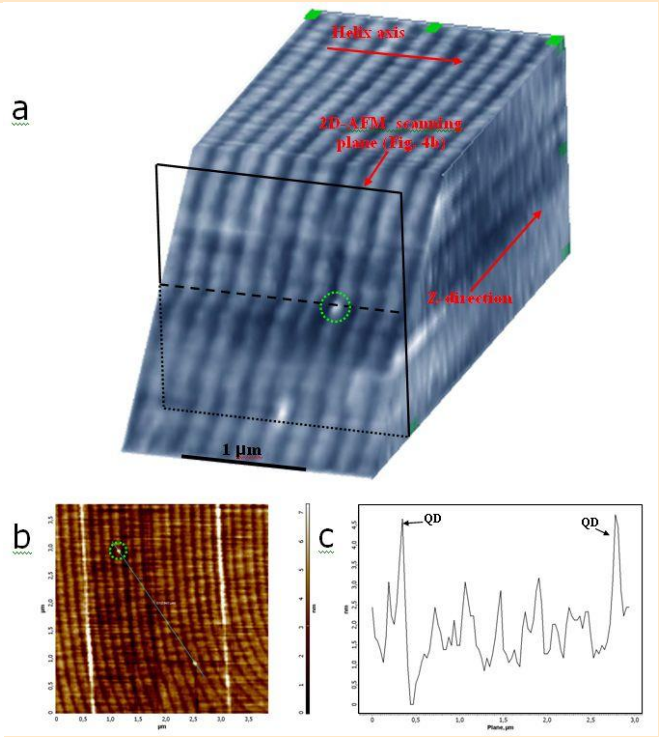

a) SPN 3D reconstruction of periodic structure of CLC-matrix doped with QD in planar zone. Z – direction is perpendicular to the cholesteric helix axis of LC-matrix. Green circle marks one of the individual QDs embedded in the matrix.
b) One of 2D AFM images used for 3D reconstruction (a), green circle marks the same individual QD that is marked on Fig. 4a.
c) Cross-section of AFM image 4b across the marked line.

Homogeneous solubility of QD in CLC-matrix w_{homo} gives a value of $(6.25\pm1.32)\cdot10^{-4}$ wt%.

SOPNT - Results

Nearfield in SOPNT is desirable when the dementions of optical features are below confocal resolution!

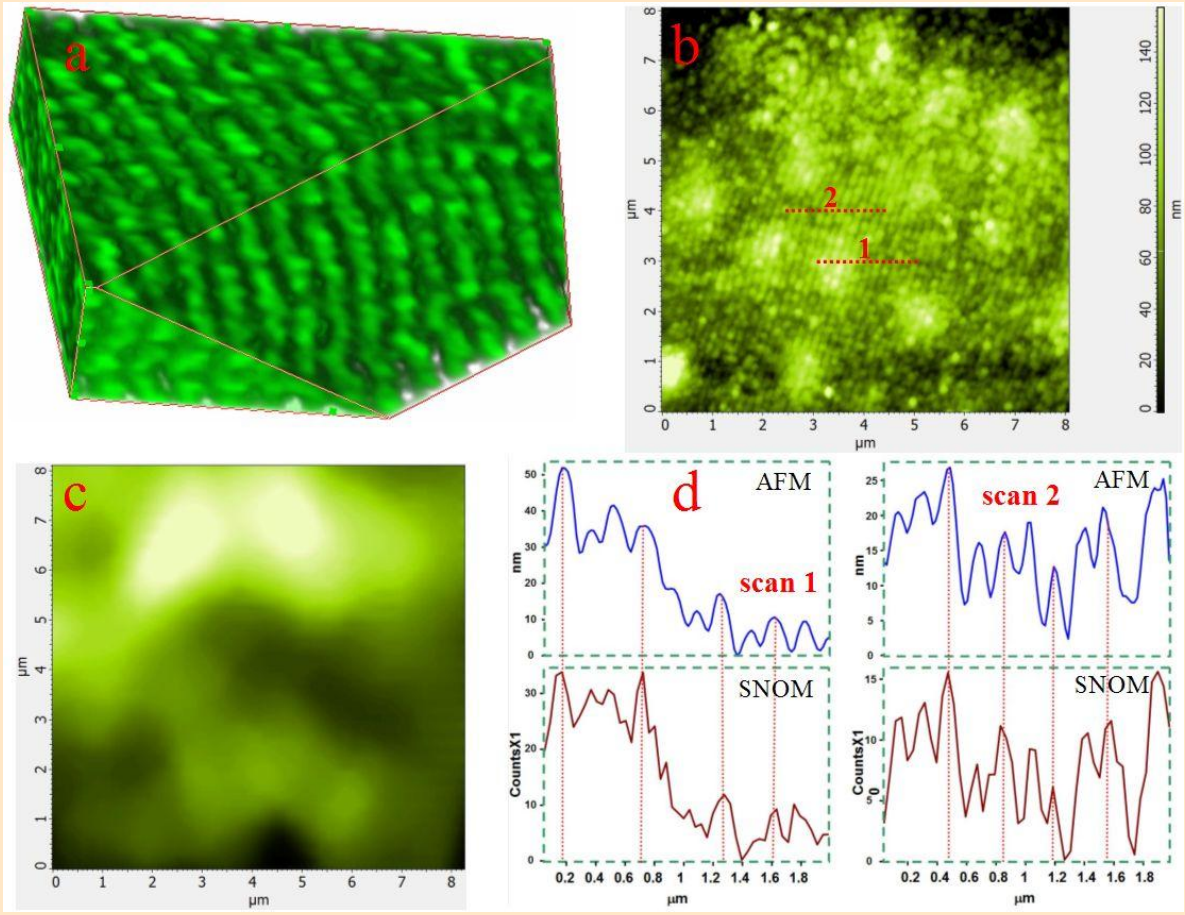

Correlation between nanoscale optical and morphological features of LC\QD materials using the 3D AFM and SNOM modes.
a) 3D AFM
b) 2D AFM of UMT-sliced sample. Lines 1 & 2 are crossections for SNOM measurement
c) Confocal fluorescent image of UMT-sliced sample.
d) The comparison of AFM and SNOM crossections from lines 1 & 2 on panel b.

SOPNT - Results

Nearfield in SOPNT is desirable when the dementions of optical features are below confocal resolution!

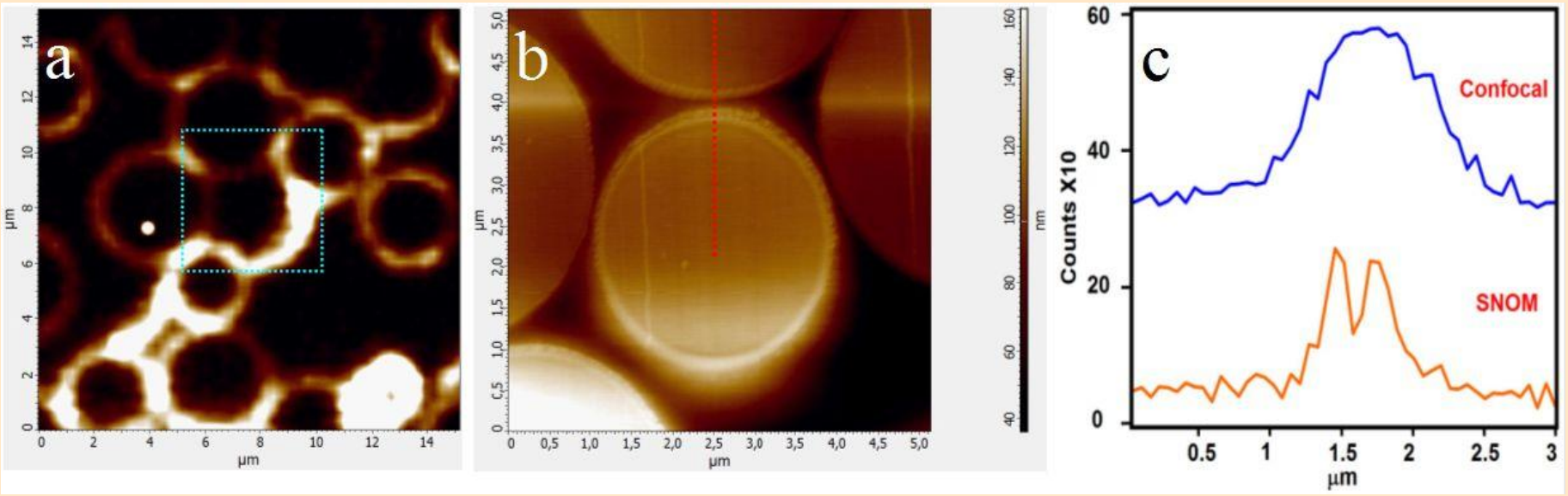

The development of characterization technique for flow cytometry fluorescent Q-beads.

a) Confocal fluorescent image of UMT-sliced sample
b) 2D AFM of UMT-sliced sample. Line is the crossections for SNOM and confocal measurements.
c) The comparison of fluorescent confocal and SNOM crossections of the line on panel b.

Main publications

1) A,E,Efimov, M.M.Moisenovich, V.G.Bogush, I.I.Agapov, 3D nanostructural analysis of silk fibroin and recombinant spidroin 1 scaffolds by scanning probe nanotomography, RSC Advances, 2014

2) K. E. Mochalov, A. E. Efimov, A. Bobrovsky, I. I. Agapov, A. A. Chistyakov, V. Oleinikov, A. Sukhanova, and I. Nabiev, Combined Scanning Probe Nanotomography and Optical Microspectroscopy: A Correlative Technique for 3D Characterization of Nanomaterials, ACS Nano, 2013, DOI: 10.1021/nn403448p

3) A. E. Efimov, H. Gnaegi, R. Schaller, W. Grogger, F. Hofer and N. B. Matsko, Analysis of native structure of soft materials by cryo scanning probe tomography, Soft Matter, 2012, 8, 9756, DOI:10.1039/c2sm26050f

4) K. E. Mochalov; A. Yu. Bobrovsky; V. A. Oleinikov; A. V. Sukhanova; A. E. Efimov; V. Shibaev; I. Nabiev, Novel cholesteric materials doped with CdSe/ZnS quantum dots with photo- and electrotunable circularly polarized emission, Proc. SPIE, 2012, 8475, Liquid Crystals XVI, 847514

5) A. Alekseev, D. Chen, E. E. Tkalya, M. G. Ghislandi, Yu. Syurik, O. Ageev, J. Loos, and G. de With Local Organization of Graphene Network Inside Graphene/Polymer Composites Adv. Funct. Mater. 2012, 22, 1311–1318

6) V.Mittal and N.B.Matsko, Tomography of the Hydrated Materials, in Analytical Imaging Techniques for Soft Matter Characterization, Engineering Materials, Springer-Verlag Berlin Heidelberg, 2012, pp. 85-93

7) A. Alekseev, A. Efimov, K. Lu, J. Loos. Three-dimensional electrical property reconstruction of conductive nanocomposites with nanometer resolution, Advanced Materials, Vol. 21, 48 (2009), pp. 4915 – 4919

8) A. Efimov, V. Sevastyanov, W. Grogger, F. Hofer, and N. Matsko. Integration of a cryo ultramicrotome and a specially designed cryo AFM to study soft polymers and biological systems, MC2009, Vol. 2: Life Sciences, p. 25, Verlag der TU Graz 2009.

9) A. E. Efimov, A. G: Tonevitsky, M. Dittrich & N. B. Matsko. Atomic force microscope (AFM) combined with the ultramicrotome: a novel device for the serial section tomography and AFM/TEM complementary structural analysis of biological and polymer samples. Journal of Microscopy, Vol. 226, Pt 3, June 2007, pp. 207–217

Nanostructures with controlled emission based on fluorescent semiconductor QD embedded in a 1D photonic crystals

Acknowledgements to The Ministry of Education and Science of The Russian Federation, grant № 14.616.21.0042

Development of 1D photonic nanostructures with photo-controlled emission based on CLC photonic matrix doped with fluorescent QD

QD/CLC systems with photovariable helix pitch:
photomodulation of photophysical properties, fluorescence and lasing.

Glass-forming cyclosiloxane matrix served as a CLC matrix SilBlue, 96.3wt%

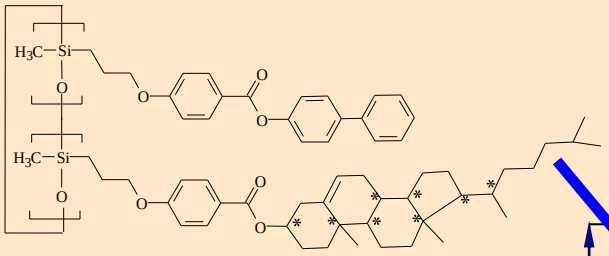

Chiral photochromic dopant Sorb, 3.2wt%

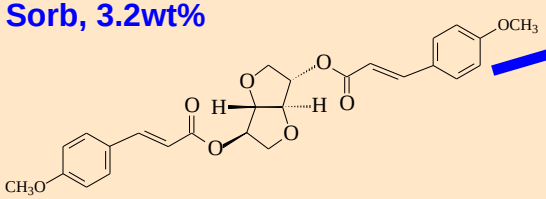

Fluorescent dopants QDs, (530 and 604 nm) 0.55wt%

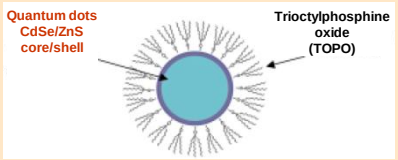

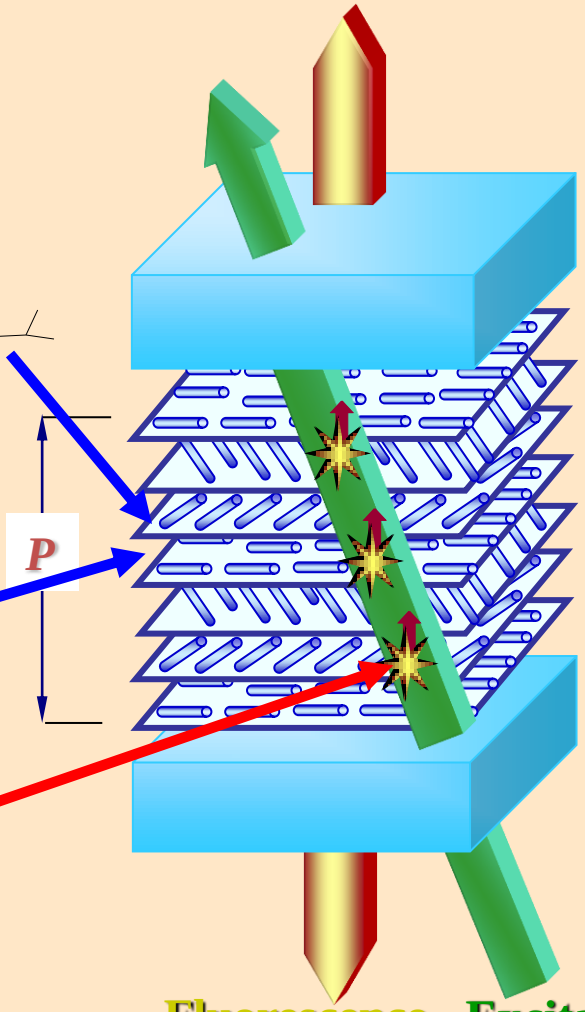

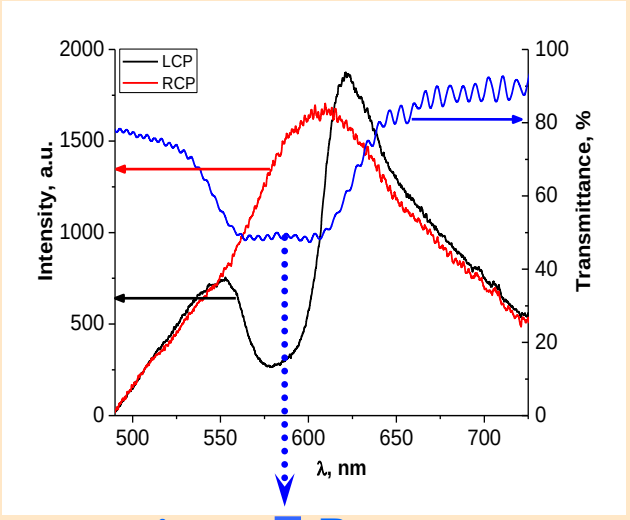

$\lambda_{max} = \bar{n} \cdot P$

P - helix pitch
n̄ - average refractive index

Development of 1D photonic nanostructures with photo-controlled emission based on CLC photonic matrix doped with fluorescent QD

*UV irradiation induces thermally irreversible E–Z isomerization of **Sorb** at C=C bonds, which is accompanied by a decrease in the helical twisting power.*

λ = 365 nm, ~2 mW/cm^2

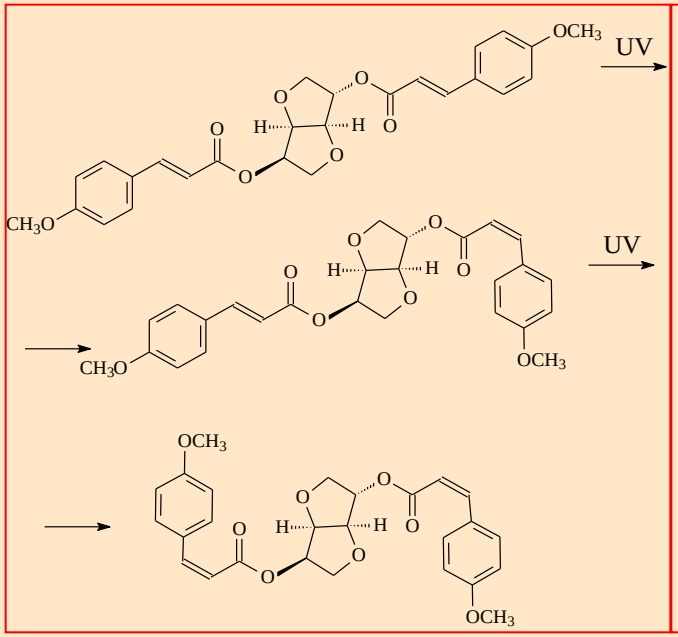

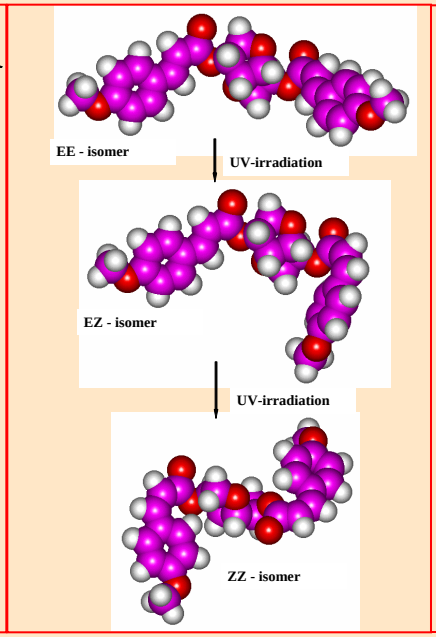

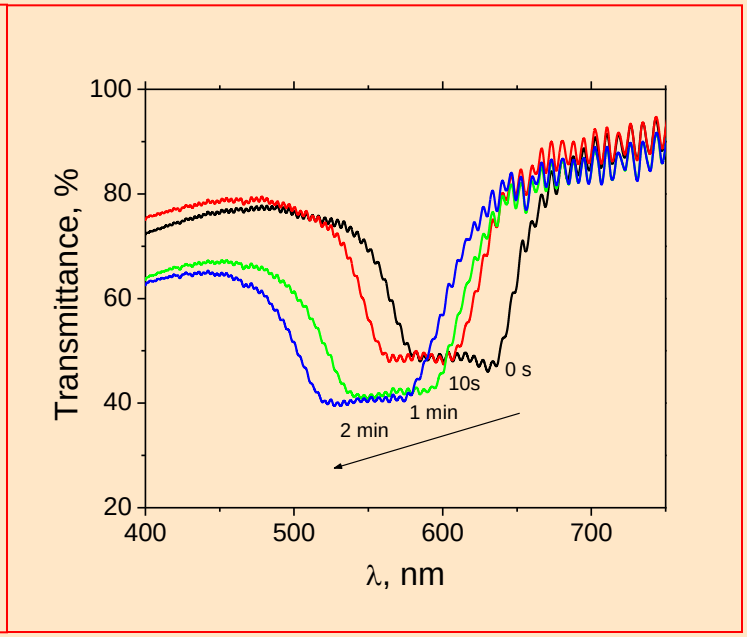

*1. Introduction of **Sorb** as a dopant into a cyclosiloxane CLC matrix leads to partial untwisting of the helix and, hence, a red shift of the selective light reflection peak.*

2. Subsequent UV irradiation results in a reverse shift of the selective light reflection peak to shorter wavelengths.

Development of 1D photonic nanostructures with photo-controlled emission based on CLC photonic matrix doped with fluorescent QD

Effect of UV-irradiation on polarization of the fluorescence of quantum dots incorporated in CLC-matrix

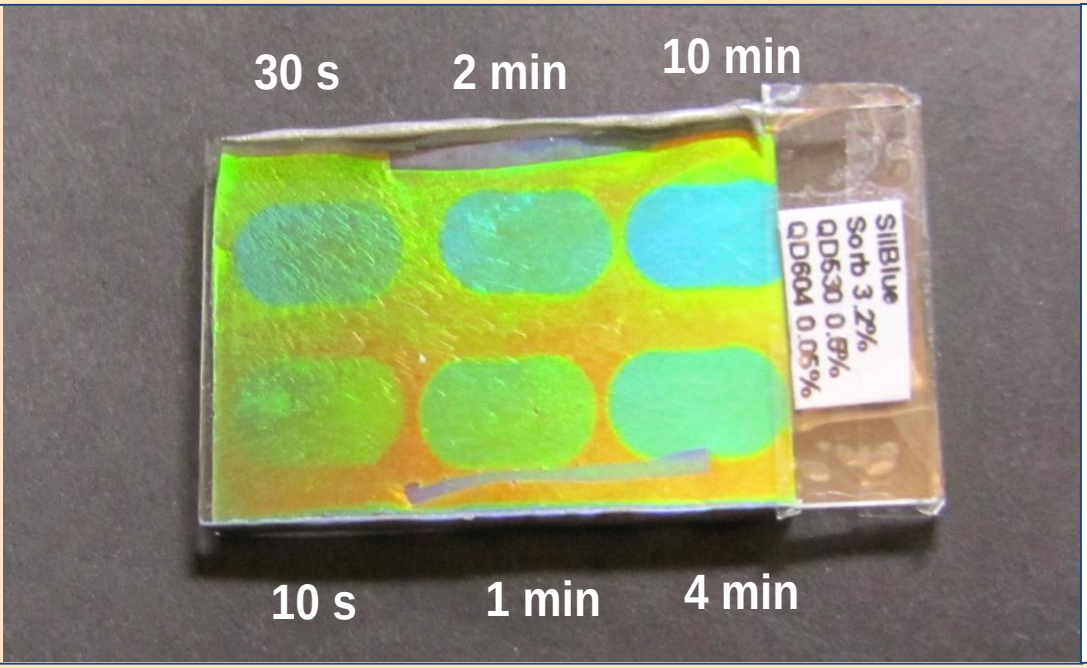

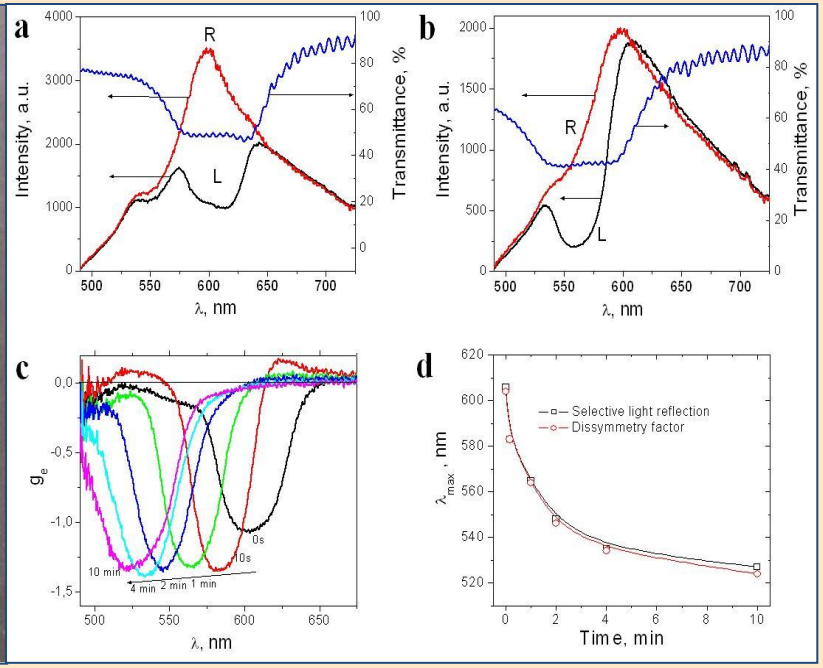

(a) Left-handed (L) and right-handed (R) circularly polarized fluorescence of QDs embedded into CLC and nonpolarized transmittance spectra of CLC before UV irradiation.
(b) The same as in (a), after 1 min of UV irradiation.
(c) Changes in the fluorescence dissymmetry factor of QDs embedded in CLC upon UV irradiation of the sample for different periods of time. $g_e = 2(I_L - I_R) / (I_L + I_R)$
(d) Dependence of the selective light reflection maximum wavelength of the CLC matrix and maximum wavelength position of the fluorescence dissymmetry factor on the duration of UV irradiation.

Development of 1D photonic nanostructures with electro-controlled emission based on CLC photonic matrix doped with fluorescent QD

Nematic LC mixture
(E-48, «Merck») (50-60%)

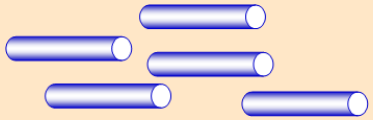

Chiral dopant
(~40%)

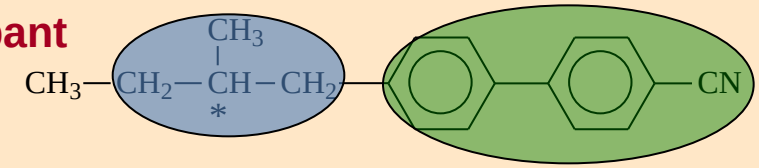

Cholesteric matrix

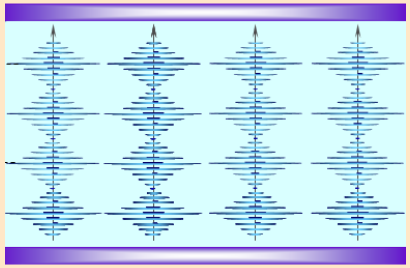

Fluorescent dopants
QDs, 604 nm) 0.55wt%

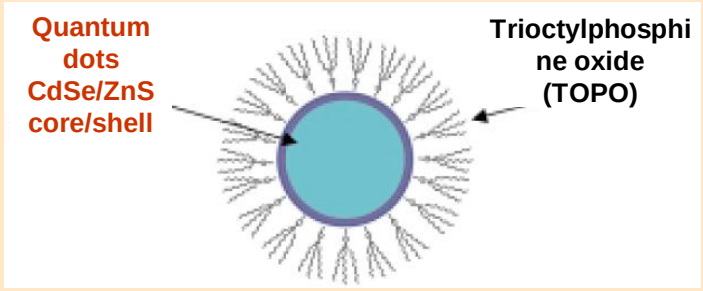

LC diacrylate (~6%)

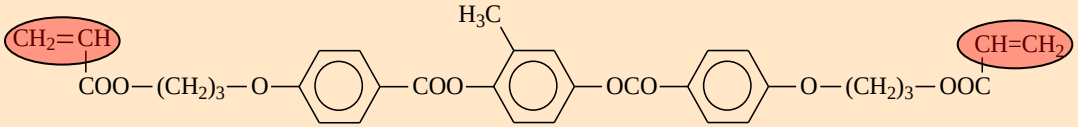

Photoinitiator(~1%)

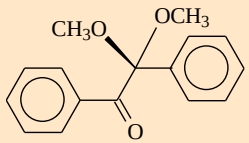

hν

(λ_{max}~335 nm)

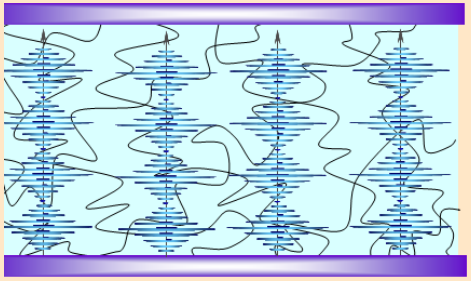

Development of 1D photonic nanostructures with electro-controlled emission based on CLC photonic matrix doped with fluorescent QD

The spectra of circularly polarized fluorescence of QD/CLC before and after application of electric field.

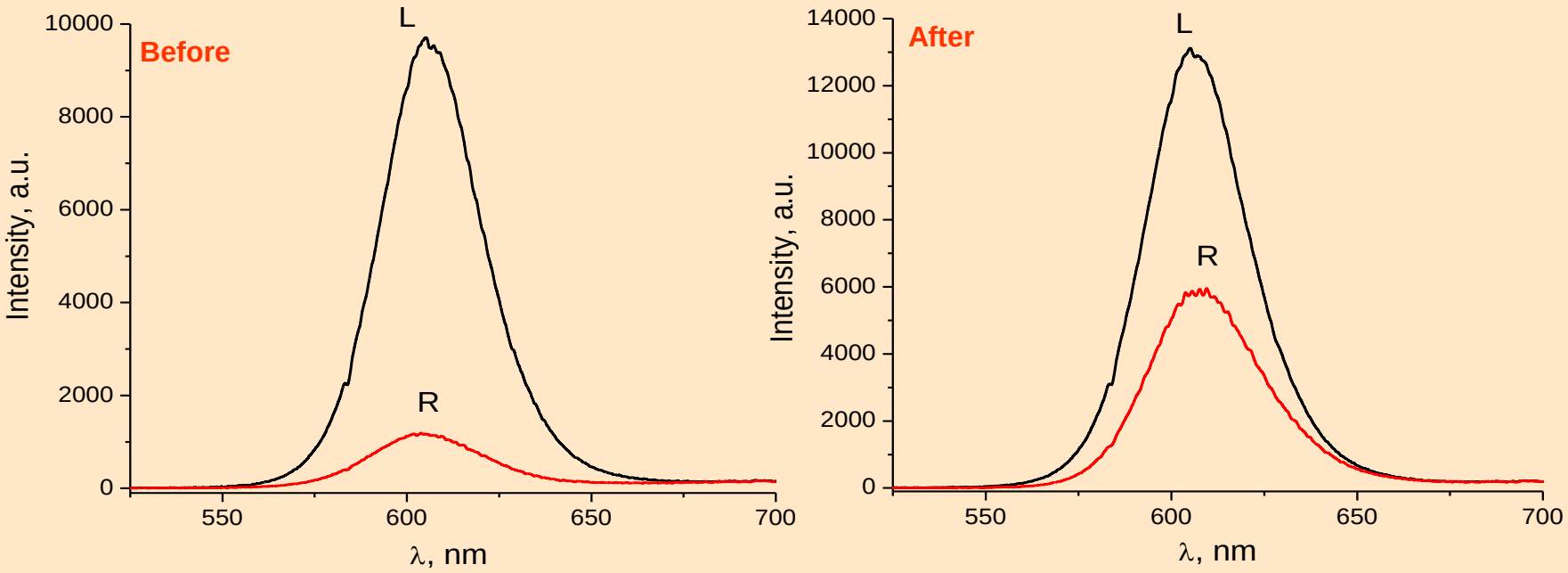

Left-handed (L) and right-handed (R) circularly polarized fluorescence spectra of CLC doped with red QDs (λ_{max} ≈ 604nm) before and after electric field application.

Application of the electric field results in a significant increase in the right-handed component contribution to the circularly polarized fluorescence emission of QDs in both QD/CLC materials. A voltage of 260 V was applied to a 20-μm cell.

Fluorescence was excited with an Ar^+ laser at λ = 488 nm with a laser power of 0.6 mW and a laser spot diameter of 2 mm.

Development of 1D photonic nanostructures with electro-controlled emission based on CLC photonic matrix doped with fluorescent QD

Effect of an electric field applied to the electrooptic cells on the fluorescence dissymmetry factors of QDs embedded in the polymer-stabilized cholesteric matrix.

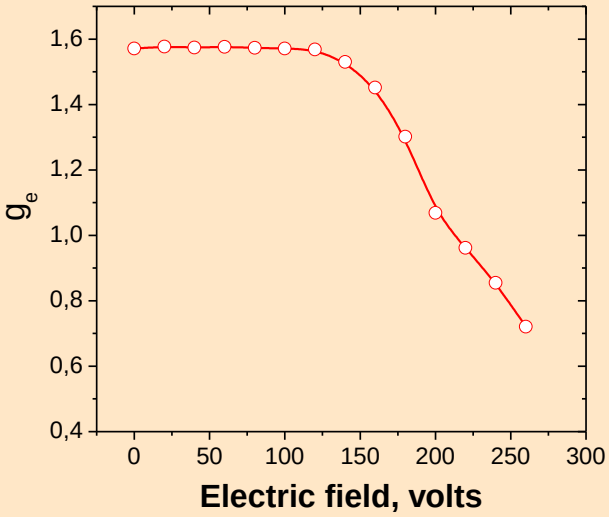

Dependence of fluorescence dissymmetry factor on electric field applied to a cell containing QD/CLC

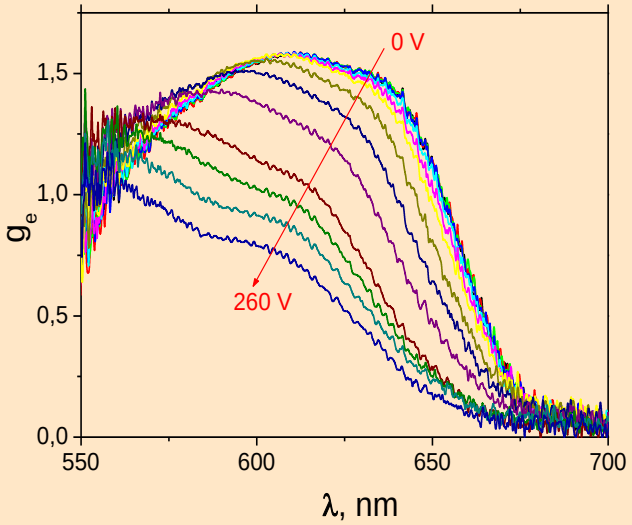

Changes in the spectral dependence of fluorescence dissymmetry factor on electric field applied to a cell containing QD/CLC. Voltage was applied at a rate of 20 volts/step

Fluorescence dissymmetry factor: $g_e = 2 (I_L - I_R) / (I_L + I_R)$

Fluorescence was excited with an Ar+ laser (λ = 488 nm) with a power of 0.6 mW and a laser spot diameter of 2 mm.

Development of 1D photonic nanostructures with controlled emission based on fluorescent QD embedded in pSi

Fabrication of porous silicon

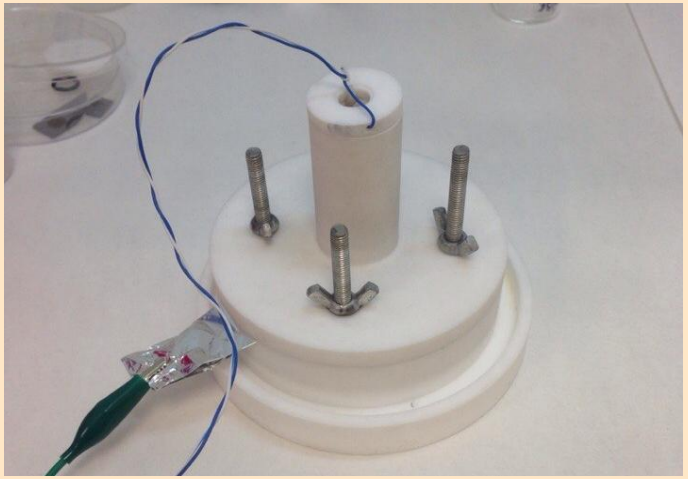

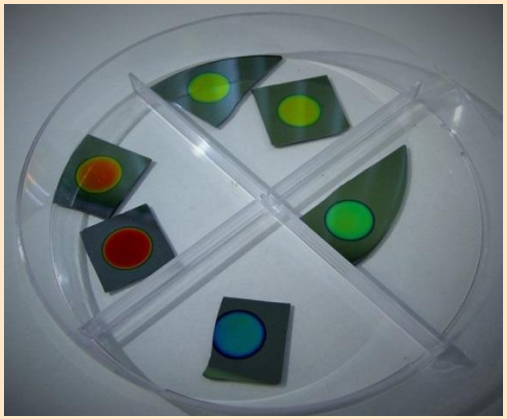

pSi based microcavities

The electrochemical etching:
The pore size ~ 30 nm
The thickness of one layer of ~ 100 nm

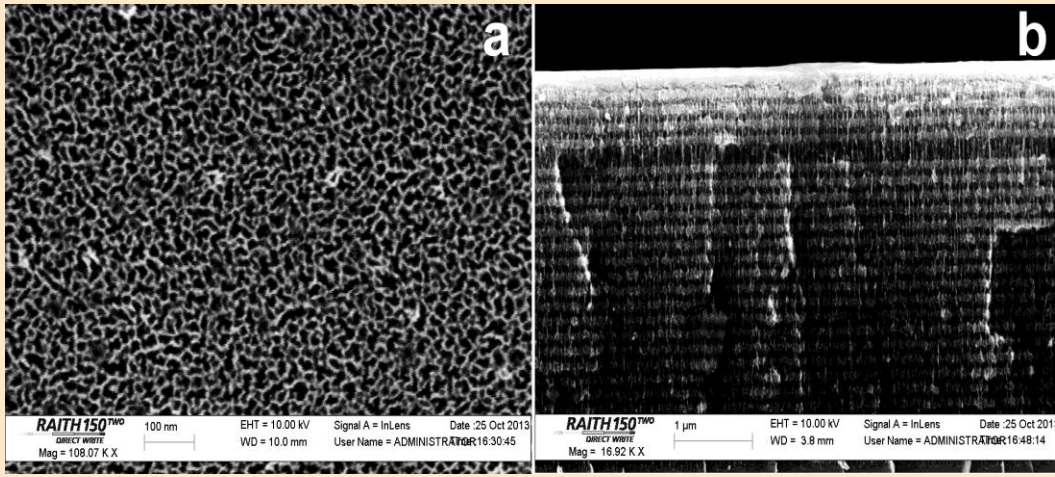

SEM images of (a) surface and (b) cleavage of the pSi microcavity

Development of 1D photonic nanostructures with controlled emission based on fluorescent QD embedded in pSi

Previous Results

The luminescence spectrum of the toluene solution of CdSe/CdS/ZnS QDs

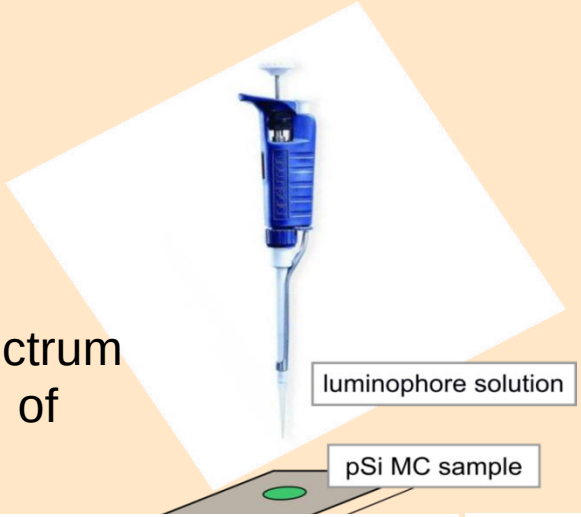

Luminescence spectrum CdSe/CdS/ZnS QDs (red) embedded in the pSi microcavity and its reflection spectrum - gray

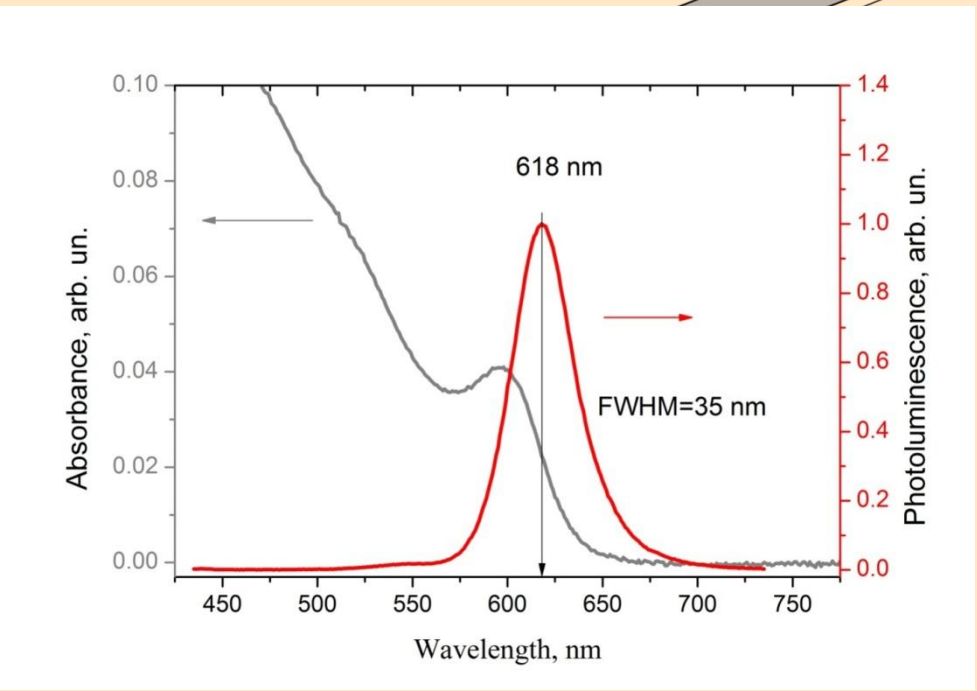

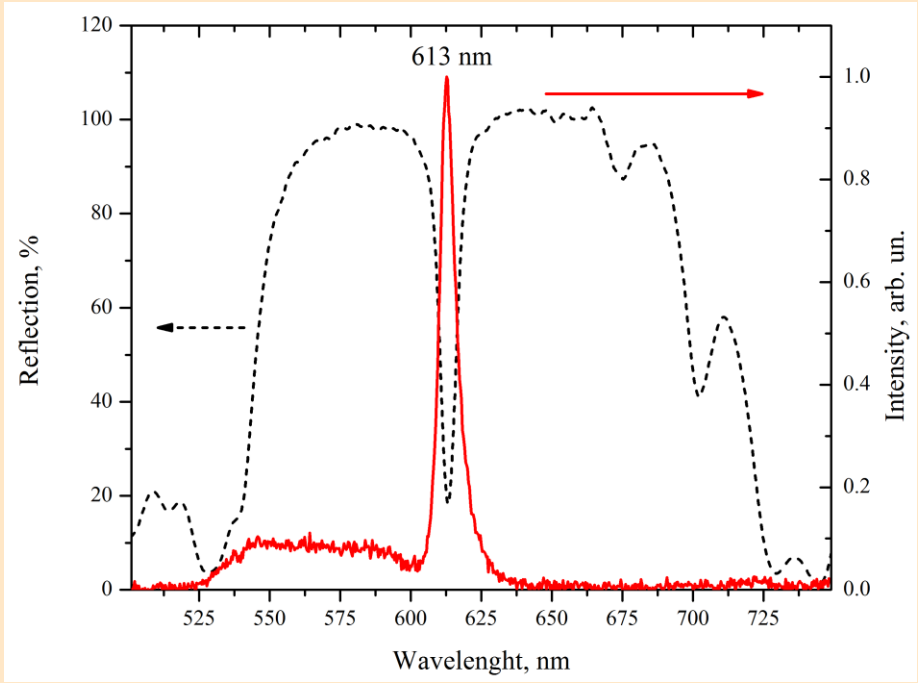

Development of 1D photonic nanostructures with controlled emission based on fluorescent QD embedded in pSi

Previous Results

Microcavity surface

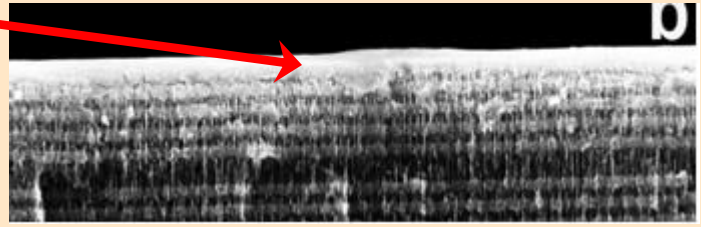

QD introduction in pSi microcavity via the capillary action

QD embedded in pSi microcavity

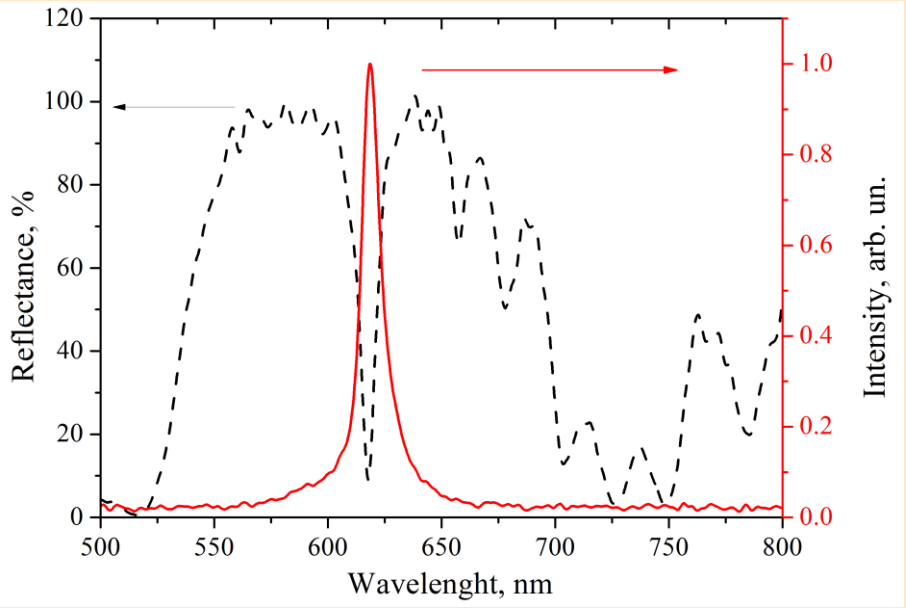

QD film on the surface of microcavity

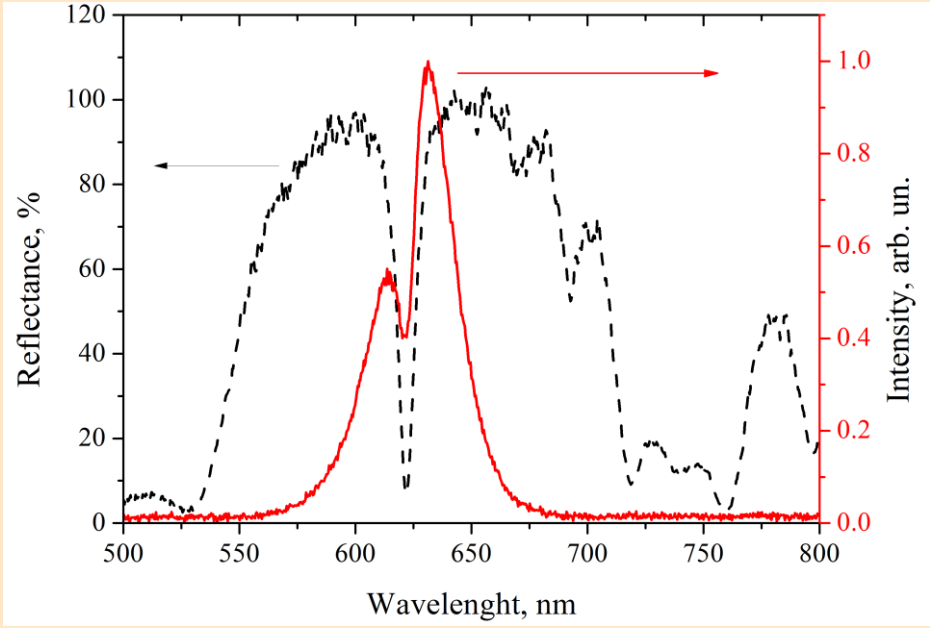

Development of 1D photonic nanostructures with controlled emission based on fluorescent QD embedded in pSi

Previous Results

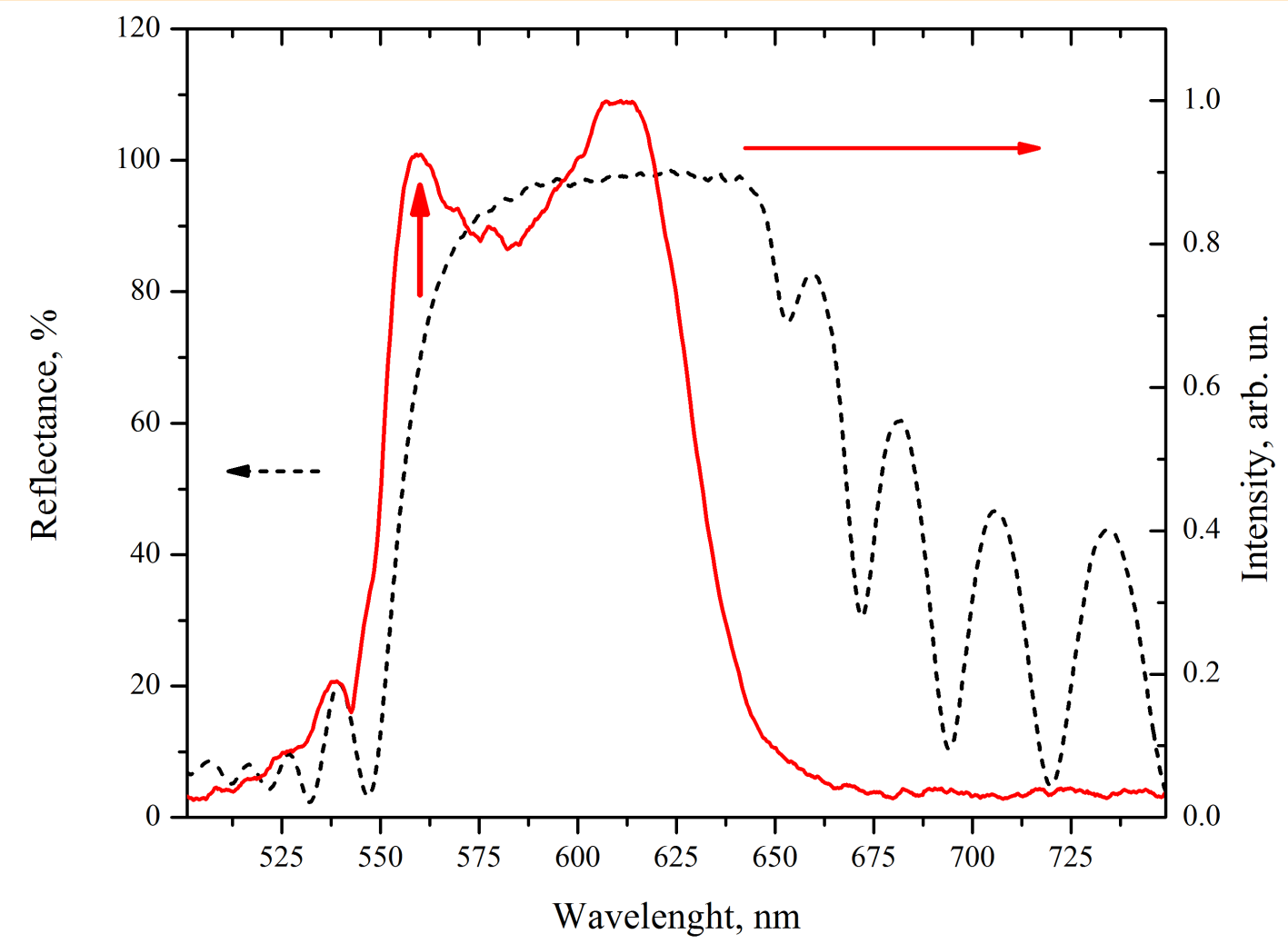

Emission of QDs embedded into a pSi Bragg mirror

Main publications

1. Zaharchenko, K.V., Obraztcova, E.A., Mochalov, K.E., Artemyev, M.V., Martynov, I.L., Klinov, D.V., Nabiev, I.R., Chistyakov, A.A., Oleinikov, V.A. Laser Physics. (2005) 15, 1150.

2. Chistyakov, A.A., Martynov, I.L., Mochalov, K.E., Oleinikov, V.A., Sizova, S.V., Ustinovich, E.A., Zakharchenko, K.V. Laser Physics. (2006) 16, 1625.

3. Chistyakov, A.A., Martynov, I.L., Mochalov, K.E., Oleinikov, V.A., Zaharchenko, K.V. Laser Physics. (2008) 18, 925.

4. Dayneko, S., Tameev, A., Tedoradze, M., Martynov, I., Artemyev, M., Nabiev, I., Chistyakov, A. Applied Physics Letters. (2013) 103, 063302.

5. Chistyakov, A.A., Dayneko, S.V., Kolesnikov, V.A., Mochalov, K.E., Oleinikov, V.A., Tedoradze, M.G., Zakharchenko, K.V. Laser Physics Letters, (2009) 6, 718.

6. Stsiapura, V., Sukhanova, A., Artemyev, M., Ustinovich, E., Strekal, N., Maskevich, S., Kulakovich, O., Mochalov, K., Nabiev, I., Oleinikov, V. Optics and Spectroscopy. (2006) 100, 854.

7. Bobrovsky, A., Mochalov, K., Chistyakov, A., Oleinikov, V., Shibaev, V. Macromolecular Chemistry and Physics. (2012) 213, 2639.

8. Bobrovsky, A., Mochalov, K., Chistyakov, A., Oleinikov, V., Shibaev, V. J. PhotochemPhotobio. A: Chemistry. (2014) 275, 30.

9. Bobrovsky, A., Mochalov, K., Oleinikov, V., Shibaev, V. Liquid Crystals. (2011) 38, 737.

10. Bobrovsky, A., Mochalov, K., Oleinikov, V., Sukhanova, A., Prudnikau, A., Artemyev, M., Shibaev, V., Nabiev, I. Advanced Materials. (2012) 24, 6216.

11. Martynov, I.L., Karavanskii, V.A., Kotkovskii, G.E., Kuzishchin, Y.A., Tsybin, A.S., Chistyakov, A.A. Technical Physics Letters. (2011) 37, 15.

12. Kotkovskiy, G.E., Kuzishchin, Y.A., Martynov, I.L., Chistyakov, A.A., Nabiev, I. Physical Chemistry Chemical Physics. (2012) 14, 13890.

13. Mochalov, K.E., Efimov, A.E., Bobrovsky, A.Y., Agapov, I.I., Chistyakov, A.A., Oleinikov, V.A., Nabiev, I. Proceedings of SPIE. (2013) 8767, 876708.

14. Mochalov, K.E., Efimov, A.E., Bobrovsky, A., Agapov, I.I., Chistyakov, A.A., Oleinikov, V., Sukhanova, A., Nabiev, I. ACS Nano. (2013) 7, 8953.

Thanks!